Available online at www.sciencedirect.com
SCIENCE DIRECT
Polymer 46 (2005) 2685–2698
polymer
www.elsevier.com/locate/polymer

Improving gas barrier of PET by blending with aromatic polyamides

Y.S. Hu[a], V. Prattipati[a], S. Mehta[b], D.A. Schiraldi[a], A. Hiltner[a,*], E. Baer[a]

[a]*Department of Macromolecular Science and Engineering, Center for Applied Polymer Research, Case Western Reserve University, Cleveland, OH 44106, USA*
[b]*INVISTA, 1551 Sha Lane, Spartanburg, SC 29304, USA*

Received 6 October 2004; received in revised form 5 December 2004; accepted 12 January 2005

Abstract

Improvement of gas-barrier properties of poly(ethylene terephthalate) (PET) by blending with an aromatic polyamide, either poly(*m*-xylylene adipamide) (MXD6) or a copolyamide based on MXD6 in which 12 mol% adipamide was replaced with isophthalamide (MXD6-12I), was studied. Incorporating a small amount of sodium 5-sulfoisophthalate into the PET matrix compatibilized the blends and reduced the polyamide domain size to 100–300 nm. Thermal analysis showed that the polyamides had a nucleating effect on PET crystallization, whereas crystallization of the polyamides was inhibited especially in compatibilized blends. Without orientation, blending with 10 wt% MXD6 or MXD6-12I reduced oxygen permeability of PET by a factor of about 0.8 (P/P_{PET}) when measured at 43% relative humidity (RH), in accordance with the Maxwell model prediction. However, after biaxial orientation, oxygen permeability of blends with 10 wt% MXD6 was reduced by 0.3 at 43% RH, and permeability of blends with 10 wt% MXD6-12I was reduced by 0.4. Even at 85% RH, oxygen permeability was reduced by 0.4 and 0.6 for blends with MXD6 and MXD6-12I, respectively. Blending with an aromatic polyamide was even more effective in reducing carbon dioxide permeability of oriented PET. Transformation of spherical polyamide domains into platelets of high aspect ratio increased tortuosity of the diffusion pathway. The platelet aspect ratio predicted by the Nielsen model was confirmed by atomic force microscopy. Higher aspect ratio of MXD6 domains was ascribed to a lower T_g compared to MXD6-12I. Similar reduction in oxygen permeability was achieved in bottle walls blown from PET blends with MXD6 or MXD6-12I.

Keywords: PET blends; Permeability; Orientation

1. Introduction

Poly(ethylene terephthalate) (PET) is widely used in the form of bottles for food-packaging because of its low cost and good mechanical properties. However, there is a continuing practical need to improve the PET gas barrier. Crystallization and orientation are two approaches to barrier enhancement, but these are limited by the processing conditions. Copolymerization offers an alternative to barrier improvement; however, the rule of mixture requires high concentration of the comonomers to achieve significant reduction in permeability, leading to increased cost.

Blending with a high barrier material is another route to decreasing permeability. Earlier work showed that blending a polyolefin with a small amount of a high barrier polymer such as a polyamide (nylon66 or nylon6) or ethylene–vinyl alcohol copolymer (EVOH) is effective in reducing gas permeability if the high barrier constituent is dispersed as platelets oriented parallel to the direction of gas flux [1–5]. Reduced permeability is achieved by increased tortuosity of the diffusion pathway.

Efforts to improve the gas barrier of PET by blending with EVOH [6], a liquid crystalline polyester [7], and aromatic polyamides [8] have been exploited. Aromatic polyamides provide higher barrier than aliphatic polyamides, and unlike aliphatic polyamides, the aromatic polyamides retain high barrier under conditions of high humidity [9], making them more suitable for beverage packaging applications [10–12]. However, achieving the optimum barrier structure of PET/polyamide blends is compromised by incompatibility of the constituent polymers.

* Corresponding author.
E-mail address: pah6@cwru.edu (A. Hiltner).

0032-3861/$ - see front matter © 2005 Elsevier Ltd. All rights reserved.
doi:10.1016/j.polymer.2005.01.056

Compatibilization strategies based on reactive blending [13], and catalytic ester–amide interchange reaction [14], can lead to crosslinking and undesirable changes in melt rheology. Incorporating a small amount of sodium 5-sulfoisophthalate into the PET matrix effectively compatibilized PET blends with aromatic polyamides by reducing the polyamide particle size [15]. Sulfonated ionomers are known to interact strongly with aliphatic polyamides, establishing a network structure with sulfonate anions coordinated to amide N–H groups and counter ions complexed to multiple amide C=O groups [16].

In the present study, PET was blended with an aromatic polyamide, either poly(*m*-xyxlylene adipamide) (MXD6) or a copolymer based on MXD6 with 12 mol% adipamide replaced with isophthalamide. The blends were compatibilized by incorporating a small amount of sodium 5-sulfoisophthalate into the PET matrix. The oxygen and carbon dioxide permeability of quenched isotropic blends and oriented blends was studied. The effects of compatibilizer content, polyamide content, conditioning RH, and testing RH on gas permeability were investigated. Structural models for gas transport were developed based on blend morphology as revealed by atomic force microscopy.

2. Materials and methods

Poly(ethylene terephthalate) (PET) and a copolymer based on polyethylene(terephthalate) with 2.29 mol% terephthalate replaced with sodium 5-sulfoisophthalate (PET-*co*-SIPE) were provided by INVISTA (Spartanburg, SC) in the form of extruded pellets. The intrinsic viscosity of the PET and PET-*co*-SIPE pellets was 0.84 and 0.56 dl g^{-1}, respectively, measured at 25 °C in dichloroacetic acid solution. Poly(*m*-xylylene adipamide) (MXD6, grade 6001, $M_n = 16{,}500$) was supplied as pellets by Mitsubishi Gas Chemical America, Inc. A copolyamide based on MXD6 in which 12 mol% of adipamide was replaced with isophthalamide (MXD6-12I) was supplied by EMS Chemie (Sumter, SC). The composition of MXD6-12I was confirmed by ^{1}H NMR using a 300 MHz Varian (Gemini 2000) FT-NMR spectrometer. The polyamides were dissolved in *d*-trifluoroacetic acid (Aldrich). The NMR spectra were run at ambient temperature. The error was $\pm 3\%$.

The PET, MXD6 and MXD6-12I pellets were dried at 120 °C for 48 h in vacuo and the compatibilizer (PET-*co*-SIPE) was dried at 80 °C in vacuo before blending. The pellets were dry blended and extruded in a Haake Rheomex TW-100 twin screw extruder with partially intermeshing, counter rotating, conical screws with converging axes. The average screw diameter was 25.4 mm and the average *L*/*D* ratio was 13:1. The barrel temperature of 285 °C and screw speed of 15 rpm were used. At the blending temperature of 285 °C, PET had lower melt viscosity than MXD6, as indicated by melt flow index measurements under similar shear rate, which favored dispersion of the MXD6 phase [17]. The melted blends were extruded through a 3 mm die, quenched in air and pelletized. The possibility of transamidation reaction between PET and MXD6 was eliminated by ^{13}C NMR analysis [15]. Blends were prepared with 5 and 10% by weight polyamide and 0, 15 and 30% by weight PET-*co*-SIPE. Transesterification during melt blending completely randomized PET and PET-*co*-SIPE to produce a homogeneous matrix copolymer. The blends are designated as wt% matrix (mol% sodium 5-sulfoisophthalate in the matrix)/wt% MXD6 or MXD6-12I.

The pellets were dried in vacuo at 80 °C for 24 h and compression-molded between Kapton sheets in a press at 270 °C to obtain films with thickness of 180–600 μm. The pellets were heated in the press for 4 min with repeated application and release of pressure to remove air bubbles, held at 309 psi (2.1 MPa) for an additional 4 min and quenched into ice water.

Compression-molded films were conditioned at 43 or 85% relative humidity (RH) and sequentially biaxially stretched in the environmental chamber of an Instron machine at a rate of 20% min^{-1}. The compression-molded film (15 cm wide, 4 cm long and 0.060 cm thick) was stretched uniaxially at 75 °C to draw ratio of 4, remounted in the grips at 90° to the first stretch and stretched again at 78 °C to achieve a final balanced biaxial draw ratio of 2.7 × 2.7. Grids were marked in the specimen for measuring the draw ratio. After drawing, the film was rapidly cooled to ambient temperature.

Two-liter carbonated soft drink bottles made from PET and PET blends were supplied by INVISTA. The bottles were blown from preforms using a commercial blow molding machine (Sidel) after the bottle preforms were conditioned at ambient RH. The side wall temperature was nominally 90 °C. The blowing cycle time was 3 s. The bottle-wall draw ratio of 2.5 × 4.0 (axial × hoop) was typical of commercial bottle production. The wall section was cut from the bottle for subsequent characterization.

Density was measured at 23 °C with a density gradient column in accordance with ASTM-D 1505 method B. The densities of PET and PET blend films were determined with a gradient made of an aqueous calcium nitrate solution and the densities of polyamide films were measured with a toluene and carbon tetrachloride gradient. Small pieces of film (~ 25 mm^2) were placed in the column and allowed to equilibrate for 30 min before the measurements were taken. The accuracy was ± 0.0009 g cm^{-3}.

Thermal analysis was conducted with a Perkin–Elmer Pyris-1 calibrated with indium and tin. Heating and cooling scans were performed under nitrogen at 10 °C min^{-1} over the temperature range from 30 to 270 °C.

The X-ray patterns of biaxially oriented films and bottle walls were recorded using a Statton camera and Ni-filtered Cu Kα radiation calibrated with calcium fluoride.

Blend morphology was examined with atomic force microscopy (AFM) using the Nanoscope IIIa MultiMode

head from Digital Instruments (Santa Barbara, CA) in the tapping mode. Specimens were microtomed at ambient temperature to expose the bulk morphology.

Oxygen flux $J(t)$ at 23 °C, 0, 43 or 85% RH, and 1 atm pressure was measured with a MOCON OX-TRAN 2/20. Carbon dioxide flux at 23 °C, 0 or 70% RH, and 1 atm pressure was measured with a MOCON PERMATRAN-C 4/40. The instrument was calibrated with NIST-certified Mylar® film of known oxygen transport characteristics. For testing at 0% RH, films were dried in vacuo. Quenched PET and blend films were dried at 60 °C and quenched MXD6 and MXD6-12I films were dried at 80 °C. Films were equilibrated in constant RH chambers before barrier testing at 43 or 85% RH. Specimens were carefully conditioned in the MOCON as described previously [18], in order to obtain the nonsteady state gas flux from which the diffusivity D was determined. To obtain the diffusivity D and to accurately determine the permeability P, the data were fit to the solution of Fick's second law with appropriate boundary conditions

$$J(t) = \frac{Pp}{l}\left[1 + 2\sum_{n=1}^{\infty}(-1)^n \exp\left(-\frac{D\pi^2 n^2 t}{l^2}\right)\right] \quad (1)$$

As indicated previously [18], the error in determining the two fitting parameters, P/l and D/l^2, was estimated not to exceed 2% for oxygen. Therefore, the accuracy of P and D was determined mainly by the accuracy of the average thickness measurement. The average thickness l of each specimen was determined as $l = w(A\rho)^{-1}$, where w is the specimen weight, A is the specimen area and ρ is the density. Solubility S was obtained from the relationship $S = PD^{-1}$.

3. Results and discussion

3.1. Blend characterization

The morphology of PET blends with 10 wt% MXD6 is shown in Fig. 1. Spherical or slightly ellipsoidal polyamide particles were dispersed in a continuous PET matrix. The uncompatibilized 90(0.00)/10 blend revealed a coarse morphology with the largest particle size of 2 μm, Fig. 1(a). The relatively large particle size confirmed the incompatibility of the two constituents. Addition of 0.38 mol% SIPE to the PET phase reduced the MXD6 particle size to 0.1–0.3 μm for in the 90(0.38)/10 blend, Fig. 1(b). Increasing SIPE further to 0.76 mol% in the PET matrix had no further effect on the particle size, Fig. 1(c). The MXD6-12I blends exhibited the same morphology as MXD6 blends at each blend composition, Fig. 1(d)–(f). Thus, incorporation of SIPE into the PET matrix effectively compatibilized the blends by reducing particle size.

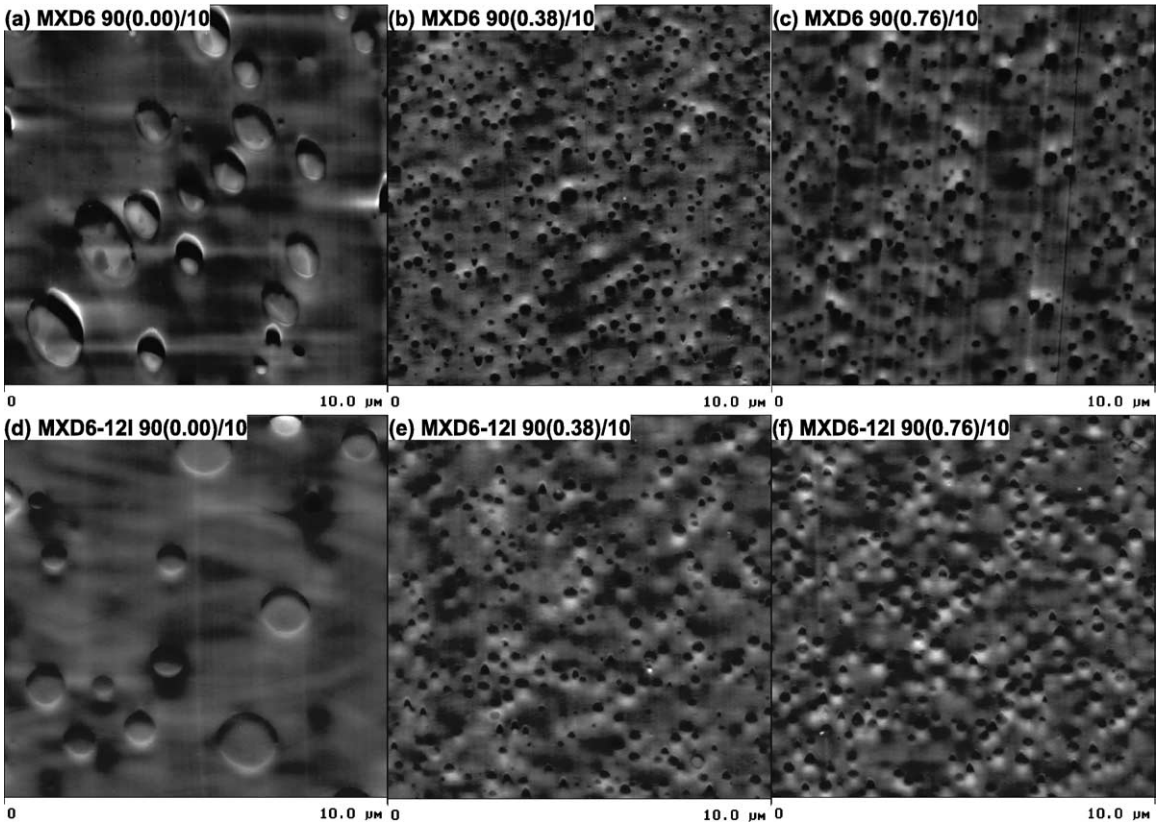

Fig. 1. AFM height images of unoriented blends: (a) 90(0.00)/10 MXD6 blend; (b) 90(0.38)/10 MXD6 blend; (c) 90(0.76)/10 MXD6 blend; (d) 90(0.00)/10 MXD6-12I blend; (e) 90(0.38)/10 MXD6-12I blend; and (f) 90(0.76)/10 MXD6-12I blend.

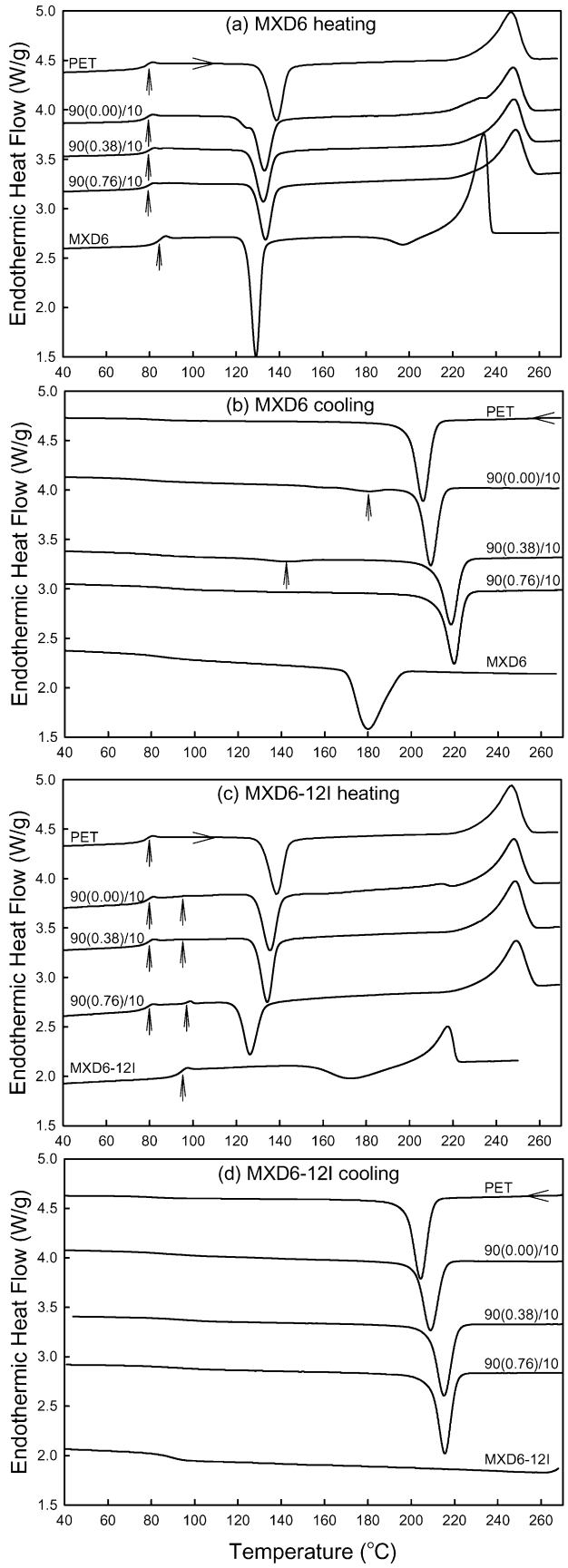

Heating and cooling thermograms of dry, compression-molded PET, MXD6, and 10 wt% MXD6 blend films with varying amounts of compatibilizer are compared in Fig. 2(a) and (b). The heating scan of PET exhibited a glass transition at 78 °C (T_g), a cold crystallization exotherm at 139 °C (T_{cc}), and a melting peak at 247 °C (T_m). Quenched MXD6 had glass transition at 84 °C, cold crystallization at 129 °C, pre-melting crystallization at 200 °C and subsequent melting at 235 °C.

As a consequence of the relatively small difference between T_g of PET and T_g of MXD6, only one inflection was detected in thermograms of their blends at a temperature corresponding to the T_g of PET. As is often the case when a second phase is added to PET [19–22], MXD6 domains nucleated crystallization as seen by the shift in T_{cc} of PET approximately 6 °C lower, Fig. 2(a). Both uncompatibilized and compatibilized blends had this effect with some scatter in T_{cc} that might have been due to small differences in quenching of the compression-molded films. The nucleation effect of MXD6 was more evident in cooling thermograms, as indicated by an increase in crystallization temperature (T_c) of 3–14 °C, Fig. 2(b). Higher T_c of compatibilized blends compared to the uncompatibilized blend was attributed to smaller domain size and larger surface area.

A shoulder at 235 °C in the heating thermogram of the 90(0.00)/10 blend corresponded to melting of MXD6. The shoulder was smaller in the 90(0.38)/10 blend and disappeared in the 90(0.76)/10 blend. In cooling scans, the crystallization temperature of the MXD6 constituent decreased and the crystallization exotherm became broader and smaller with increasing amount of compatibilizer until MXD6 crystallization completely disappeared for the 90(0.76)/10 blend, Fig. 2(b). Hindrance and inhibition of MXD6 crystallization were ascribed to fractionated crystallization behavior as a result of the small droplet size (100–300 nm) and strong interaction between SIPE and MXD6. A detailed analysis was presented previously [15].

Thermograms of MXD6-12I, and blend films with 10 wt% MXD6-12I and varying amounts of compatibilizer are shown in Fig. 2(c) and (d). The heating scan of MXD6-12I exhibited T_g of 93 °C, which was higher than the T_g of MXD6 due to the incorporation of isophthalamide. A broad cold crystallization exotherm centered at 173 °C immediately preceded the melting endotherm at 218 °C, Fig. 2(c). Higher T_{cc} and lower T_m of MXD6-12I compared to MXD6 reflected the effect of kinked isophthalamide groups on crystallization rate and crystal order, respectively. Correspondence in the enthalpies of cold crystallization and melting indicated that the quenched MXD6-12I film was amorphous. The cooling curve showed no crystallization

Fig. 2. Thermal analysis of quenched and dry blends: (a) heating thermograms of MXD6 blends; (b) cooling thermograms of MXD6 blends; (c) heating thermograms of MXD6-12I blends; and (d) cooling thermograms of MXD6-12I blends.

Table 1
Thermal analysis of dry PET, MXD6, MXD6-12I and their blends

Material and composition		Heating						Cooling	
		T_g (°C)	T_{cc} (°C)	ΔH_{cc} (J g^{-1})	T_m (°C)	ΔH_m (J g^{-1})	ϕ_c	T_c (°C)	ΔH_c (J g^{-1})
Controls	PET	78	139	35	247	41	0.05	205	44
	MXD6	84	129, 200	40, 7	235	55	–	180	56
	MXD6-12I	93	173	22	218	22	0	–	0
MXD6 blends	90(0.00)/10	78	124, 133	32	233, 248	40	–	208, 180	42, 4
	90(0.38)/10	78	133	32	248	39	0.06	218, 140	44, 2
	90(0.76)/10	78	134	30	249	39	0.07	219	42
MXD6-12I blends	90(0.00)/10	78, 93	136, 165	33	215, 248	39, 2	0.05	208	40
	90(0.38)/10	78, 93	136	32	248	39	0.06	214	40
	90(0.76)/10	78, 95	126	30	248	41	0.09	215	41

exotherm, only the T_g at the same temperature as in the heating scan, Fig. 2(d).

Appearance of two distinct inflections in thermograms of MXD6-12I blends, which corresponded to the T_gs of the constituents, indicated immiscibility of PET and MXD6-12I. Crystallization of PET in the blends was accelerated by the nucleating effect of MXD6-12I, as evidenced by a decrease in T_{cc} and an increase in T_c. A small endotherm in the heating thermogram of the 90(0.00)/10 blend at 215 °C corresponded to melting of MXD6-12I. The MXD6-12I melting peak was absent in heating scans of the compatibilized blends.

The thermal transition temperatures and corresponding enthalpies for the constituent polymers and their blends are compiled in Table 1. For uncompatibilized blends, in which both PET and the polyamide crystallized, total heat of melting and heat of melt crystallization of the constituents were close to the additive predictions. For compatibilized blends, in which polyamide did not crystallize, ΔH_m and ΔH_c were attributable to PET only. A slight difference between the heat of melting (ΔH_m) and heat of cold crystallization (ΔH_{cc}) represented a small amount of weight crystallinity ϕ_c ($\sim$6% based on ΔH_o of 125 J g^{-1} [23]) in quenched PET and PET blend films.

3.2. Oxygen transport properties of PET and polyamides

Typical experimental curves in Fig. 3 describe the oxygen flux $J(t)$ through quenched PET, MXD6 and MXD6-12I films tested at 23 °C and 43% RH. In order to facilitate comparisons among specimens that varied somewhat in thickness, the flux data were normalized to a film thickness of 200 μm using Eq. (1) with P and D calculated from the original film thickness. The initial increase in oxygen flux reflected nonsteady-state diffusion. This part of the curve was controlled mainly by the diffusivity D. As the permeant concentration in the specimen reached a constant distribution, the flux reached the steady-state value J_o. This value,

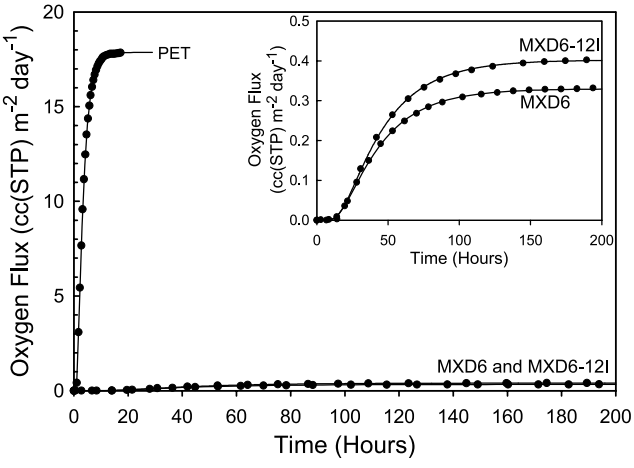

Fig. 3. Experimental $J(t)$ data for unoriented PET, MXD6 and MXD6-12I tested at 23 °C, 43% RH and the fit to Eq. (1).

Table 2
Effect of RH on oxygen transport parameters of PET, MXD6 and MXD6-12I

Material	RH (%)	Water sorption (%)	T_g (°C)	Density (g cm^{-3})	P	D	S
PET	0	0	78	1.3379	0.360	4.8	0.087
	43	0.2	76	–	0.363	5.2	0.081
	85	0.6	71	–	0.390	6.4	0.070
MXD6	0	0	84	1.1965	0.0199	0.54	0.043
	43	3.7	48	1.2050	0.0067	0.40	0.019
	85	6.0	<23	1.2196	0.0089	0.96	0.011
MXD6-12I	0	0	93	1.2059	0.0232	0.52	0.049
	43	3.3	54	1.2131	0.0080	0.39	0.024
	85	9.5	18	1.2104	0.0295	2.0	0.017

P—[cc(STP) cm m^{-2} atm^{-1} day^{-1}], D—[10^{-13} m^2 s^{-1}], S—[cc(STP) cm^{-3} atm^{-1}].

normalized to the film thickness l and the permeant gas pressure p, defined the permeability $P = J_o l p^{-1}$.

Comparison of flux curves indicated that MXD6 and MXD6-12I had a much longer nonsteady-state region (slower diffusion) and much lower steady-state plateau value (lower permeability) than PET. The fit to the solution of Fick's second law (Eq. (1)) is included with the experimental points in Fig. 3. The fit was equally good for all the experiments in the study. The two fitting parameters P/l and D/l^2 were used to obtain diffusivity D and to accurately determine the permeability P. Solubility S was calculated from the relationship $S = PD^{-1}$.

Oxygen transport characteristics of quenched PET, MXD6 and MXD6-12I tested at various RH are listed in Table 2. At 0% RH, oxygen permeability of MXD6 and MXD6-12I was 16–18 times lower than that of PET, due to extremely low D and somewhat lower S. Comparing the two polyamides, D was about the same for MXD6 and MXD6-12I, the slightly higher P of MXD6-12I was due to higher S, which reflected the higher T_g of MXD6-12I.

Increasing RH from 0 to 85% increased P of PET only slightly. A substantial increase in D was largely offset by a decrease in S. In contrast to PET, permeability of polyamides changed significantly with RH. Oxygen permeability decreased by a factor of about 0.3 for both MXD6 and MXD6-12I as RH increased from 0 to 43%. Decreases in P were due to decreases in both D and S, with S decreasing more than D. Reduction in S was due to the drop of T_g, whereas the decrease in D was attributed to suppression of the γ-relaxation by crosslink effect of tightly bound water [9,24]. At 85% RH, loosely bound water was incorporated into existing hydrogen bonds between amide groups in all polyamides, which weakened the intermolecular cohesion [9,24]. Also, both MXD6 and MXD6-12I were rubbery at the testing temperature of 23 °C, and P increased because of an increase in D. Nevertheless, the polyamides retained much lower permeability than PET. Lower P of MXD6 compared to MXD6-12I at high RH, by about a factor of 0.3, was due to crystallization [9,25].

Sequential biaxial orientation of PET to 2.7×2.7 decreased P from 0.363 to 0.253 cc(STP) cm m^{-2} atm^{-1} day^{-1}, Table 3. This result was obtained by conditioning PET at 43% RH before orientation. Conditioning PET at 85% RH before orientation resulted in slightly lower P. In contrast to PET, sequential biaxial orientation after conditioning at 43% RH did not improve barrier of MXD6 and MXD6-12I. Indeed, P increased due to an increase in S. This somewhat surprising effect of orientation on permeability of MXD6 was reported previously [26], and might be due to disruption of hydrogen bonds during orientation [27]. A slight decrease in density was consistent with the increase in S.

3.3. Oxygen transport properties of unoriented blends

Oxygen flux $J(t)$ through quenched PET and 90(0.38)/10 blends tested at 23 °C and 43% RH is shown in Fig. 4 with the flux normalized to a film thickness of 200 μm. The flux

Table 3
Effect of biaxial orientation (2.7×2.7) on oxygen transport parameters of PET, MXD6 and MXD6-12I measured at 43% RH

Material	Density (g cm^{-3})	P	D	S
PET	1.3379	0.363	5.2	0.081
PET oriented[a]	1.3544	0.253	4.3	0.069
PET oriented[b]	1.3547	0.242	4.1	0.068
MXD6	1.2050	0.0067	0.40	0.019
MXD6 oriented[a]	1.2034	0.0112	0.46	0.028
MXD6-12I	1.2131	0.0080	0.39	0.024
MXD6-12I oriented[a]	1.2116	0.0095	0.38	0.029

P—[cc(STP) cm m^{-2} atm^{-1} day^{-1}], D—[10^{-13} m^2 s^{-1}], S—[cc(STP) cm^{-3} atm^{-1}].
[a] Conditioned at 43% RH before orientation.
[b] Conditioned at 85% RH before orientation.

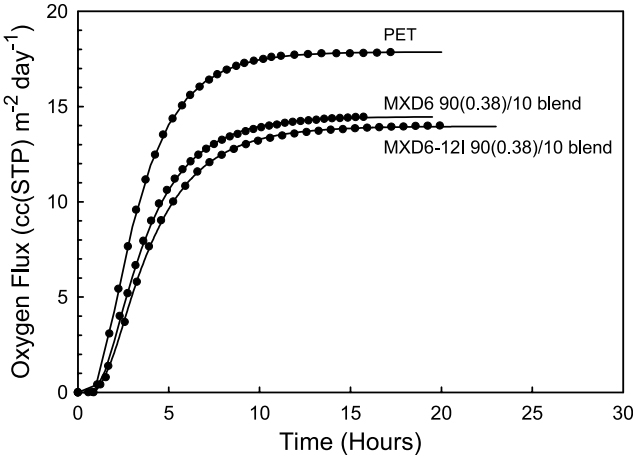

Fig. 4. Experimental $J(t)$ data for unoriented blends tested at 23 °C, 43% RH and the fit to Eq. (1).

curves of blends with MXD6 and MXD6-12I were about the same, and compared to PET, the nonsteady-state region broadened (slower diffusion) and the steady-state flux decreased (lower permeability). The oxygen transport properties of isotropic PET and PET blends with 10 wt% MXD6 or MXD6-12I and varying amounts of compatibilizer are summarized in Table 4. At 43% RH, blending with 10 wt% MXD6 decreased P of PET by about 0.83. The decrease in P was almost entirely due to a decrease in D. Compatibilizing the blend decreased P only slightly more. Blending with MXD6-12I had essentially the same effect as blending with MXD6.

Unlike P and D, which depend on blend morphology, S should depend only on blend composition, and should equal the additive contributions of the blend constituents. Using data for PET and polyamides from Table 2, S was calculated to be 0.074 and 0.075 cc(STP) cm^{-3} atm^{-1} for PET blends with 10 wt% (11 vol% from density) MXD6 and MXD6-12I, respectively, in excellent agreement with the experimental results, Table 4.

The effect of testing RH was examined with the 90(0.38)/10 blend composition, Table 5. Like PET, P of MXD6 and MXD6-12I blends increased only slightly as RH increased from 0 to 85%. The change was due to an increase in D. Blending with 10 wt% polyamide decreased P of PET by about the same amount regardless of testing RH.

Blend permeability was compared to predictions of the Maxwell model for a dispersion of spherical particles of lower permeability in a continuous matrix of higher permeability [28]

$$\frac{P}{P_{PET}} = \left[1 + \frac{3\phi_{PA}}{\frac{(P_{PA}/P_{PET})+2}{(P_{PA}/P_{PET})-1} - \phi_{PA}}\right] \quad (2)$$

where P_{PET} is permeability of the continuous PET phase, P_{PA} is permeability of the dispersed polyamide phase, and ϕ_{PA} is the volume fraction of dispersed phase and equals 0.11 for blends with 10 wt% polyamide. Taking P_{PET} from Table 2 as 0.363 cc(STP) cm m^{-2} atm^{-1} day^{-1}, and P_{PA} as either 0.0067 for MXD6 or 0.0080 cc(STP) cm m^{-2} atm^{-1} day^{-1} for MXD6-12I, Eq. (2) predicts a decrease in permeability at 43% RH (P/P_{PET}) of 0.84 for both polyamides. The decrease in P at 0 and 85% RH predicted by Eq. (2) is 0.84–0.86 based on data in Table 2. This is very close to the prediction of 0.84 assuming the polyamide to be impermeable ($P_{PA}=0$), and in fairly good agreement with the experimental value of about 0.80, Table 5.

3.4. Oxygen transport properties of biaxially oriented blends

The X-ray diffraction patterns of biaxially oriented films are shown in Fig. 5. Relatively sharp arcs on the meridian revealed strain-induced crystallization caused by the first draw. These arcs were (010) reflections superposed on $(0\bar{1}1)$ reflections [29]. Diffuse arcs on the equator revealed the mixed orientation of amorphous phase and crystalline phase parallel to the second draw [29,30]. The blend films gave virtually the same X-ray diffraction pattern as PET.

The AFM phase images in Fig. 6 show cross-sections of oriented 90(0.38)/10 blend films. The image in Fig. 6(a) shows highly elongated MXD6 domains oriented in the plane of the film. The MXD6 platelets were about 35 nm thick and 1.0–1.8 μm long. The platelets in the MXD6-12I blend of the same composition were slightly thicker, about 50–90 nm, and shorter, 0.9–1.6 μm long, Fig. 6(b). Apparently MXD6-12I did not draw as readily as MXD6 because of the higher T_g, 54 °C for MXD6-12I compared to 48 °C for MXD6 at 43% RH.

The effect of blending on oxygen flux $J(t)$ through

Table 4
Effect of compatibilizer content on oxygen transport parameters of PET blends measured at 43% RH

Material and composition		Density (g cm^{-3})	P	D	S	P/P_{PET}
PET		1.3379	0.363	5.2	0.081	1.00
MXD6 blends	90(0.00)/10	1.3256	0.303	4.5	0.078	0.83
	90(0.38)/10	1.3258	0.295	4.6	0.075	0.81
	90(0.76)/10	1.3266	0.298	4.4	0.078	0.82
MXD6-12I blends	90(0.00)/10	1.3221	0.295	4.5	0.076	0.81
	90(0.38)/10	1.3237	0.282	4.3	0.076	0.78
	90(0.76)/10	1.3258	0.289	4.4	0.076	0.80

P—[cc(STP) cm m^{-2} atm^{-1} day^{-1}], D—[10^{-13} m^2 s^{-1}], S—[cc(STP) cm^{-3} atm^{-1}].

Table 5
Effect of RH on oxygen transport parameters of PET blends

Material and composition	Density (g cm^{-3})	RH (%)	P	D	S	P/P_{PET}
PET	1.3379	0	0.360	4.8	0.087	1.00
		43	0.363	5.2	0.081	1.00
		85	0.390	6.2	0.073	1.00
MXD6 90(0.38)/10 blend	1.3258	0	0.271	4.0	0.079	0.75
		43	0.295	4.6	0.075	0.81
		85	0.318	5.3	0.065	0.82
MXD6-12I 90(0.38)/10 blend	1.3237	0	0.272	3.8	0.083	0.76
		43	0.282	4.3	0.076	0.78
		85	0.314	5.3	0.069	0.81

P—[cc(STP) cm m^{-2} atm^{-1} day^{-1}], D—[10^{-13} m^2 s^{-1}], S—[cc(STP) cm^{-3} atm^{-1}].

biaxially oriented PET films tested at 23 °C and 43% RH is shown in Fig. 7 with the flux normalized to a film thickness of 200 μm. Comparison of flux curves for blends with 5 and 10 wt% polyamide indicated blending affected both the nonsteady-state and steady state parts of the oxygen flux curve. The nonsteady-state region broadened (slower diffusion) and the steady-state flux decreased (lower permeability) significantly compared to PET. Comparison of flux curves for MXD6 and MXD6-12I blends indicated a broader nonsteady-state region and decreased steady-state flux for the MXD6 blends.

Biaxial orientation reduced P of the blends dramatically, for example from 0.295 to 0.078 cc(STP) cm m^{-2} atm^{-1} day^{-1} for the 90(0.38)/10 blend with MXD6 at 43% RH, Tables 5 and 6. Moreover, biaxial orientation decreased P of the blends much more than P of PET. In the same example, the value of P/P_{PET} was 0.81 for the unoriented blend, but decreased to 0.31 for the oriented blend, Tables 5 and 6. The dramatic decrease in P/P_{PET} was achieved by transformation of spherical polyamide domains into platelets oriented perpendicular to the oxygen flux. The increased tortuousity of the diffusion pathway resulted in a sizable decrease in D. Similarly, blends with MXD6-12I exhibited much lower P/P_{PET} than the unoriented blend. Because the polyamides had about the same D at 43% RH, somewhat higher P/P_{PET} values for MXD6-12I blends suggested that MXD6-12I domains had lower aspect ratio than MXD6 domains. Solubility followed the additive contributions of the blend constituents based on results for oriented PET and polyamides in Table 3.

The effect of testing RH on the barrier properties of biaxially oriented blends was studied with the 90(0.38)/10 composition, Table 7. In contrast to P of oriented PET, which increased only slightly between 0 and 85% RH, P of the oriented 90(0.38)/10 MXD6 blend changed from 0.120 to 0.078 to 0.121 cc(STP) cm m^{-2} atm^{-1} day^{-1} as RH increased from 0 to 43 to 85%, respectively. The corresponding changes in P/P_{PET} were 0.48, 0.31 and 0.46. The same trend was observed with the oriented 90(0.38)/10 MXD6-12I blend and other blend compositions with 5 and 10 wt% MXD6 or MXD6-12I. The minimum in P/P_{PET} at 43% RH paralleled the minimum in P of the polyamides at 43% RH (Table 2), and indicated that the polyamide domains were not completely impermeable, especially at low and high RH. Crystallization of MXD6 was not a consideration for the small domains in compatibilized blends.

The effect of conditioning the films at 85% RH before orientation, rather than 43% RH, was examined with biaxially oriented blends with 10% MXD6-12I, Table 8.

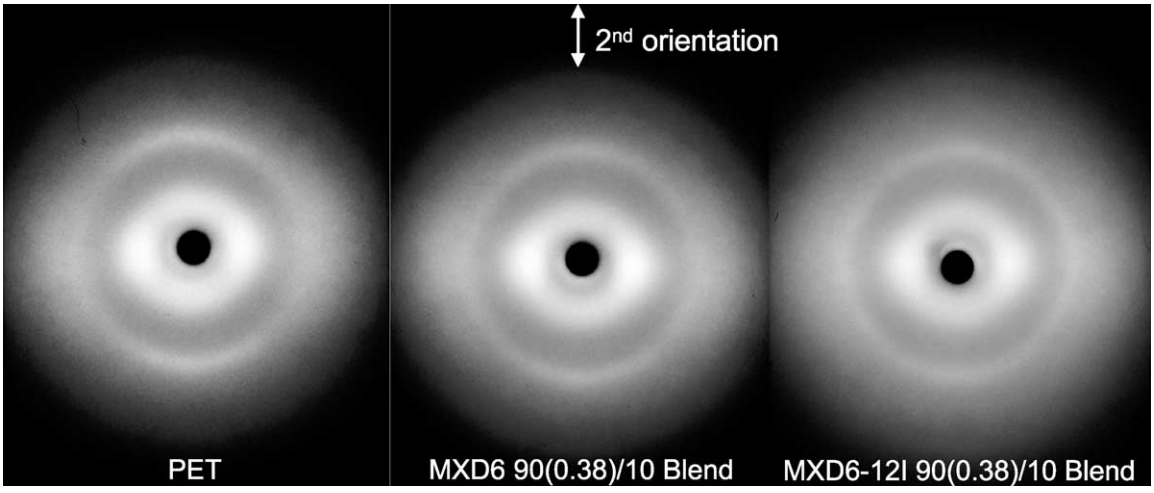

Fig. 5. X-ray patterns for biaxially oriented blend films: (a) PET; (b) 90(0.38)/10 MXD6 blend; and (c) 90(0.38)/10 MXD6-12I blend.

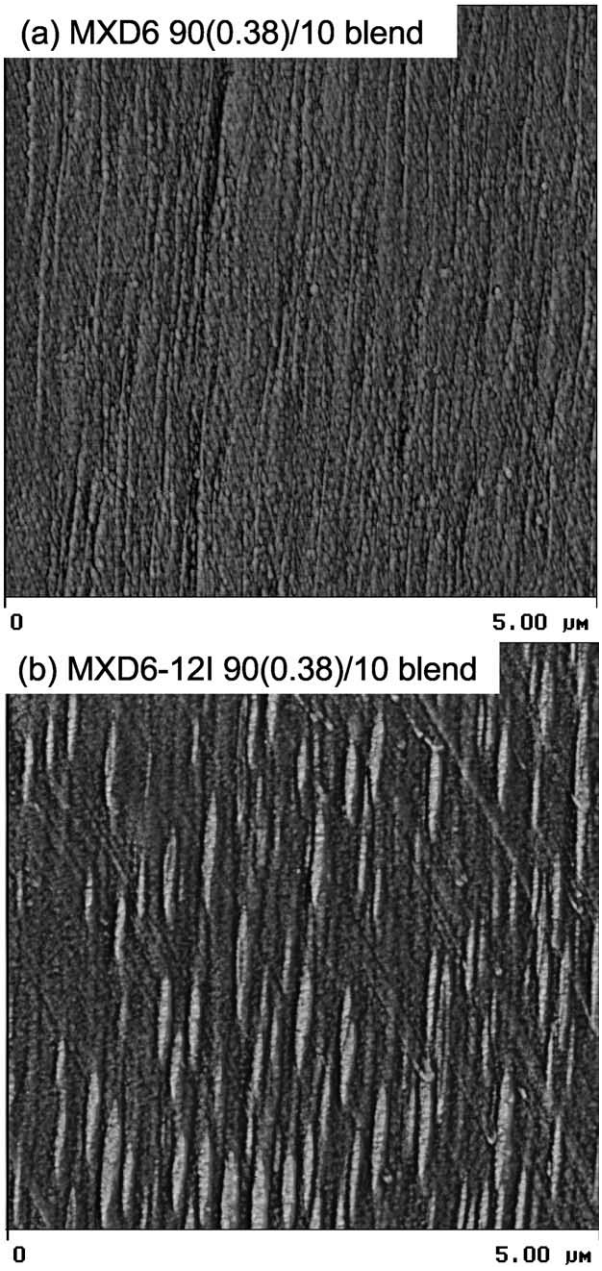

Fig. 6. AFM phase images of biaxially oriented blend films: (a) 90(0.38)/10 MXD6 blend and (b) 90(0.38)/10 MXD6-12I blend.

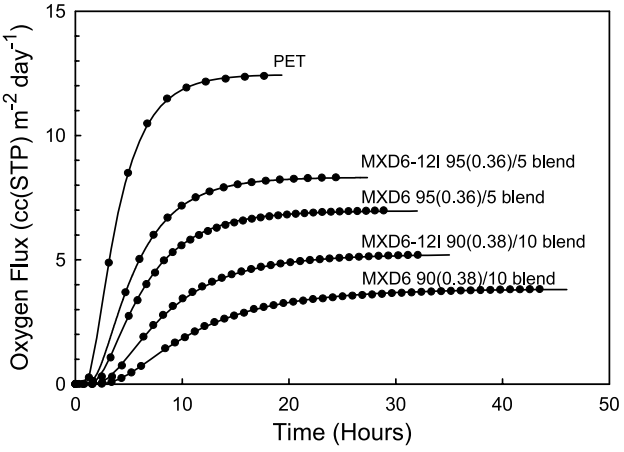

Fig. 7. Experimental $J(t)$ data for biaxially oriented blends tested at 23 °C, 43% RH and the fit to Eq. (1).

Compatibilization had virtually no effect on P of oriented blends that were conditioned at 43% RH. For all compositions, P was about 0.104 cc(STP) cm m^{-2} atm^{-1} day^{-1}. However, conditioning at 85% RH increased P of the uncompatibilized blend to 0.137 cc(STP) cm m^{-2} atm^{-1} day^{-1}. Void formation, as evidenced by whitening of stretched films, was responsible for the increase in P. At 85% RH, T_g was low enough that MXD6-12I readily crystallized at the orientation temperature of 75 °C. Possibly, crystallization of the relatively large MXD6-12I particles together with poor adhesion to PET led to interfacial debonding during stretching of the uncompatibilized blend. In this regard, it is noted that MXD6 crystallized even more readily than MXD6-12I in the uncompatiblized blend. The same phenomenon was reported previously in the uncompatibilized MXD6 blend conditioned at 43% RH [15]. In contrast to the uncompatibilized MXD6-12I blend, conditioning at 85% RH decreased P of the compatibilized blends to about 0.090 cc(STP) cm m^{-2} atm^{-1} day^{-1}. The small particle size in the compatibilized blends prevented crystallization of MXD6-12I. Good adhesion to PET together with decreased T_g, from 54 °C at 43% RH to 18 °C at 85% RH, facilitated drawing of the polyamide domains to high aspect ratio during orientation.

The Nielsen model describes the change in P produced by a dispersion of platelets with orientation perpendicular to

Table 6
Effect of blend composition on oxygen transport parameters of biaxially oriented (2.7×2.7) PET blends measured at 43% RH

Material and composition		Density (g cm^{-3})	P	D	S	P/P_{PET}	Aspect ratio (Eq. (3))
PET		1.3544	0.253	4.3	0.069	1.00	–
MXD6 blends	95(0.36)/5	1.3471	0.142	2.7	0.060	0.56	25
	90(0.38)/10	1.3406	0.078	1.5	0.060	0.31	34
MXD6-12I blends	95(0.36)/5	1.3502	0.169	3.1	0.064	0.67	15
	90(0.38)/10	1.3437	0.104	1.9	0.063	0.41	22

Conditioned at 43% RH before orientation. P—[cc(STP) cm m^{-2} atm^{-1} day^{-1}], D—[10^{-13} m^2 s^{-1}], S—[cc(STP) cm^{-3} atm^{-1}].

Table 7
Effect of RH on oxygen transport parameters of biaxially oriented (2.7×2.7) PET blends

Material and composition	Density (g cm^{-3})	RH (%)	P	D	S	P/P_{PET}	Aspect ratio (Eq. (3))
PET	1.3544	0	0.251	3.9	0.074	1.00	–
		43	0.253	4.3	0.069	1.00	–
		85	0.264	4.5	0.068	1.00	–
MXD6 90(0.38)/10 blend	1.3406	0	0.120	2.0	0.069	0.48	–
		43	0.078	1.5	0.060	0.31	34
		85	0.121	2.4	0.058	0.46	–
MXD6-12I 90(0.38)/10 blend	1.3437	0	0.155	2.5	0.072	0.62	–
		43	0.104	1.9	0.063	0.41	22
		85	0.160	3.0	0.062	0.61	–

Conditioned at 43% RH before orientation. P—[cc(STP) cm m^{-2} atm^{-1} day^{-1}], D—[10^{-13} m^2 s^{-1}], S—[cc(STP) cm^{-3} atm^{-1}].

the gas flux [31]

$$\frac{P}{P_{PET}} = \frac{1-\phi_{PA}}{1+\alpha\frac{\phi_{PA}}{2}} \quad (3)$$

where α is the platelet aspect ratio. For a given particle volume fraction polyamide, the relative permeability is only a function of aspect ratio according to Eq. (3). The oriented blends came closest to fulfilling the Nielsen assumption of an impermeable dispersed phase when tested at 43% RH, where both the polyamides alone and the corresponding oriented blends had the lowest value of P. The quantity P/P_{PET} is plotted versus ϕ_{PA} in Fig. 8 for 95(0.36)/5 and 90(0.38)/10 MXD6 and MXD6-12I blends conditioned at 43% RH, taking P_{PET} as 0.253 cc(STP) cm m^{-2} atm^{-1} day^{-1}, Table 8. A good fit of Eq. (3) to data for MXD6 blends was obtained with aspect ratio of 27. For platelets about 35 nm thick, the corresponding length would be 1.0 μm, which is consistent with the platelet dimensions in the AFM image, Fig. 6(a).

A good fit of Eq. (3) to data for MXD6-12I blends conditioned at 43% RH was obtained with aspect ratio of 18. The lower aspect ratio of MXD6-12I domains was consistent with the AFM image that showed platelets about 70 nm thick and 1.3 μm long, Fig. 6(b). Lower aspect ratio of MXD6-12I domains was attributed to greater difficulty in drawing the higher T_g polyamide. Data are also included for 90(0.38)/10 and 90(0.76)/10 MXD6-12I blends conditioned at 85% RH in order to reduce T_g. It should be noted that films conditioned at 85% RH were exposed to lower RH during orientation and probably some amount of water was lost in the process. Taking P_{PET} as 0.242 cc(STP) cm m^{-2} atm^{-1} day^{-1} for blends conditioned at 85% RH, Table 8, increasing the conditioning RH from 43 to 85% resulted in oriented films with P/P_{PET} closer to the Nielsen curve for MXD6 blends with aspect ratio of 27.

The maximum aspect ratio achievable by balanced biaxial orientation of spherical particles is determined by the biaxial draw ratio λ. Assuming that the spherical domains deform affinely into circular disks of equal volume, the maximum aspect ratio can be estimated as $3/2\lambda^3$. The maximum aspect ratio of the platelet produced by 2.7×2.7 biaxial orientation is 30, which is only slightly larger than the value of 27 obtained from the Nielsen model as applied to oriented MXD6 blends conditioned at 43% RH and MXD6-12I blends conditioned at 85% RH.

The lower limit for P of the blends is given by a series arrangement of infinite PET and polyamide layers

$$\frac{1}{P} = \frac{1-\phi_{PA}}{P_{PET}} + \frac{\phi_{PA}}{P_{PA}} \quad (4)$$

where P_{PET} is taken as 0.253 cc(STP) cm m^{-2} atm^{-1} day^{-1} for blends conditioned at 43% RH, and P_{PA}, the permeability of biaxially oriented polyamide at 43% RH, is taken as 0.0112 and 0.0095 cc(STP) cm m^{-2} atm^{-1} day^{-1} for MXD6 and MXD6-12I, respectively, Table 3.

Table 8
Effect of conditioning RH on oxygen transport parameters of biaxially oriented (2.7×2.7) PET blends with MXD6-12I measured at 43% RH

Composition	Conditioning RH (%)	Density (g cm^{-3})	P	D	S	P/P_{PET}	Aspect ratio (Eq. (3))
PET	43	1.3544	0.253	4.3	0.069	1.00	–
	85	1.3547	0.242	4.1	0.068	1.00	–
90(0.00)/10	43	1.3405	0.107	1.9	0.065	0.42	22
	85	1.3195	0.137	1.8	0.088	0.57	11
90(0.38)/10	43	1.3437	0.104	1.9	0.063	0.41	22
	85	1.3390	0.095	1.7	0.065	0.39	25
90(0.76)/10	43	1.3437	0.103	1.9	0.063	0.41	22
	85	1.3377	0.090	1.6	0.065	0.37	27

P—[cc(STP) cm m^{-2} atm^{-1} day^{-1}], D—[10^{-13} m^2 s^{-1}], S—[cc(STP) cm^{-3} atm^{-1}].

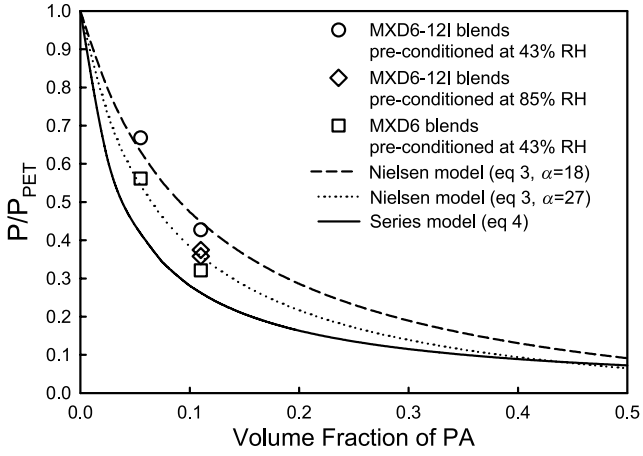

Fig. 8. P/P_{PET} as a function of volume fraction of polyamides and fit to Eq. (3).

Eq. (4) gives P/P_{PET} of 0.30 and 0.26 for MXD6 and MXD6-12I blends with 10 wt% (11 vol%) polyamide. The limit for MXD6-12I blends is included in Fig. 8, and is closely approached by the blends with P/P_{PET} of 0.31.

3.5. Oxygen transport properties of blend bottle walls

The X-ray diffraction pattern of the bottle walls is shown in Fig. 9. The longer, sharper meridional arcs of higher intensity revealed more organized crystals and higher crystallinity in bottle walls than in biaxially oriented films. The arcs, (010) superposing on $(0\bar{1}1)$ reflections, showed greater orientation in the hoop direction than in the axial direction of the bottle wall [29,32]. Diffuse arcs on the meridian revealed the orientation of amorphous phase parallel to the hoop direction. The blend bottle walls gave virtually the same pattern as PET.

The AFM phase images in Fig. 10 show cross-sections cut in the hoop direction of bottle walls blown from 90(0.38)/10 blends. Platelet-shaped polyamide domains are oriented parallel to bottle walls. The MXD6 platelets were about 40 nm thick and 1.0–1.6 μm long. The MXD6-12I platelet had thickness of 50–60 nm and length of 1.0–1.4 μm. The polyamide platelets in bottle walls appeared somewhat thinner than in biaxially oriented blend films.

The oxygen barrier properties of 2-liter blend bottle walls with 95(0.36)/5 and 90(0.38)/10 compositions are given in Table 9. The results for biaxially oriented films of the same compositions tested under the same conditions are given in Table 6. At 43% RH, bottle walls showed somewhat lower P than the biaxially oriented films due to lower D. This was due to higher crystallinity in bottle walls as indicated by higher density and sharper crystalline X-ray reflections with stronger intensity. However the effect of blending as measured by P/P_{PET} was similar for bottle walls and oriented films. Considering 90(0.38)/10 blends with MXD6, P/P_{PET} was 0.36 for bottle walls compared to 0.31 for oriented films. In both bottle walls and oriented films, MXD6-12I was less effective than MXD6 for reducing P. The P/P_{PET} values were 0.45 for bottle walls and 0.41 for oriented films for the 90(0.38)/10 blend. Correspondence in permeability reduction between bottle walls and oriented films meant that the polyamide domains in bottle walls had about the same effective aspect ratio as the polyamide domains in 2.7×2.7 oriented film.

The draw ratio of bottle walls is approximately 2.5×4.0 (axial×hoop). The maximum aspect ratio estimated from the transformation of polyamide spheres in preforms to elliptical discs in bottle walls is 38 as defined by the smaller radius of the ellipse. This is considerably larger than the effective aspect ratio of about 27 for bottle walls calculated from Eq. (3) for MXD6 blends. This contrasts with oriented films where the aspect ratio achieved with MXD6 blends is close to the maximum value of 30 for 2.7×2.7 biaxial orientation. Based on the given draw ratios, the blend bottle walls have considerable potential for higher particle aspect ratio and lower P/P_{PET}. Possibly the polyamides do not draw as well at the high rate used for blowing bottles as they

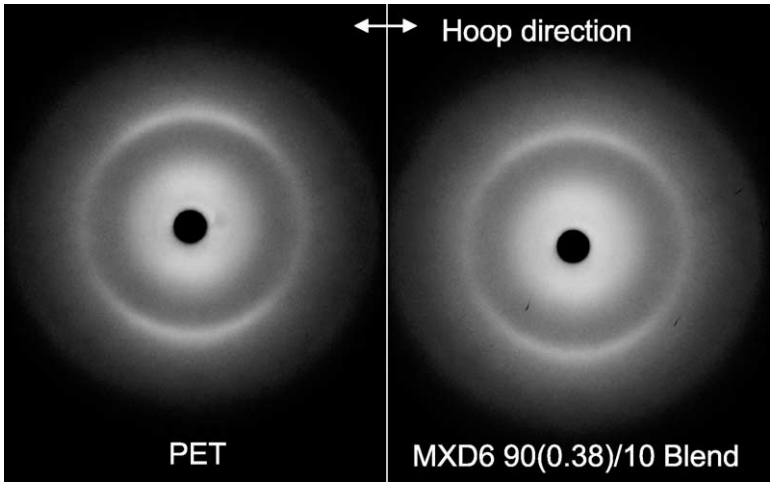

Fig. 9. X-ray patterns for bottle walls: (a) PET and (b) 90(0.38)/10 MXD6 blend.

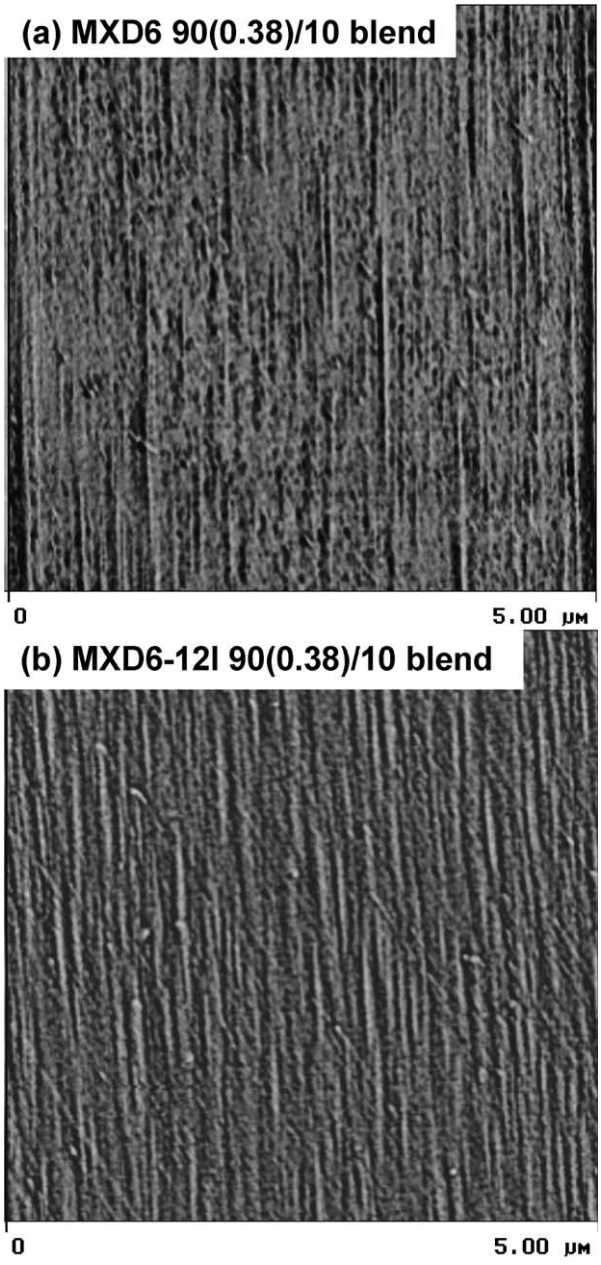

Fig. 10. AFM phase images of blend bottle walls: (a) 90(0.38)/10 MXD6 blend; and (b) 90(0.38)/10 MXD6-12I blend.

do at the lower rate used in biaxial film orientation. Nevertheless, the predictive capability of biaxially oriented films should be underlined.

3.6. Carbon dioxide transport properties of blends

Carbon dioxide and oxygen transport parameters measured at 0% RH are compared in Table 10. In all cases, P for carbon dioxide (P_{CO2}) exceeded P for oxygen (P_{O2}). Although D_{CO2} was actually lower than D for oxygen, much higher S_{CO2} compared to S for oxygen was responsible for higher P_{CO2}. The effect of blending on P_{CO2} paralleled the trend observed with P_{O2}. Thus, P/P_{PET} of unoriented 90(0.38)/10 blends was about the same, 0.77–0.80, for both CO_2 and O_2. Accordingly, the ratio P_{CO2}/P_{O2} of 4 for PET was preserved with the blends.

Biaxial orientation of PET reduced P_{CO2} and P_{O2} by the same factor, thereby preserving the ratio P_{CO2}/P_{O2} of 4. The ratio P_{CO2}/P_{O2} for biaxially oriented MXD6 and MXD6-12I was considerably lower, 2.7 for MXD6 and 2.2 for MXD6-12I. The unexpectedly low value of P_{CO2} for oriented polyamides was due to D rather than S. Values of the ratio P_{CO2}/P_{O2} less than 4 were previously observed for other polar polymers [33,34], and can be attributed to interaction of the polar CO_2 molecule with polar groups on the polymer.

Qualitatively, biaxial orientation of the blends had the same effect on P_{CO2} as on P_{O2}. Thus, biaxially oriented 90(0.38)/10 blends had lower P/P_{PET} than 95(0.36)/5 blends; and orientation was more effective in reducing P/P_{PET} of MXD6 blends than of MXD6-12I blends with the same composition. However, P/P_{PET} values for oriented blends were consistently lower for carbon dioxide than for oxygen. This meant that the platelet blend morphology reduced carbon dioxide permeation more than predicted by the ratio P_{CO2}/P_{O2} of 4. Indeed, the ratio for oriented blends was 3.2–3.5. Lower P_{CO2}/P_{O2} ratio of the oriented blends compared to oriented PET reflected the impact of polyamide properties on the gas transport properties of the blend.

Effect of testing RH on the transport parameters of carbon dioxide was examined with biaxially oriented MXD6 films at 70% RH, Table 11. In contrast to P_{CO2} of oriented PET, which increased only slightly between 0 and 70% RH, P_{CO2} of the oriented 90(0.38)/10 MXD6 blend

Table 9
Effect of blend composition on oxygen transport parameters of bottle walls measured at 43% RH

Material and composition		Density (g cm^{-3})	P	D	S	P/P_{PET}	Aspect ratio (Eq. (3))
PET		1.3704	0.180	3.1	0.067	1.00	–
MXD6 blends	95(0.36)/5	1.3595	0.099	1.7	0.067	0.55	26
	90(0.38)/10	1.3519	0.065	1.2	0.063	0.36	27
MXD6-12I	95(0.36)/5	1.3617	0.126	2.2	0.065	0.70	13
blends	90(0.38)/10	1.3539	0.081	1.5	0.062	0.45	18

P—[cc(STP) cm m^{-2} atm^{-1} day^{-1}], D—[10^{-13} m^2 s^{-1}], S—[cc(STP) cm^{-3} atm^{-1}].

Table 10
Comparison of carbon dioxide and oxygen transport parameters of biaxially oriented (2.7×2.7) PET blends measured at 0% RH

Material	Composition	Carbon dioxide				Oxygen				P_{CO2}/P_{O2}
		P	D	S	P/P_{PET}	P	D	S	P/P_{PET}	
PET	Unoriented	1.37	1.04	1.53	1.00	0.360	4.8	0.087	1.00	3.8
PET	Oriented	0.96	0.83	1.34	1.00	0.251	3.9	0.074	1.00	3.8
MXD6	Oriented	0.061	0.070	1.00	0.06	0.023	0.45	0.061	0.09	2.7
MXD6-12I	Oriented	0.047	0.055	0.97	0.05	0.022	0.41	0.061	0.09	2.2
MXD6 blends	90(0.38)/10 unoriented	1.10	0.84	1.52	0.80	0.271	4.0	0.079	0.75	4.1
	90(0.38)/10 oriented	0.39	0.38	1.20	0.41	0.120	2.0	0.069	0.48	3.3
	95(0.36)/5 oriented	0.54	0.50	1.25	0.56	0.170	2.9	0.068	0.68	3.2
MXD6-12I blends	90(0.38)/10 unoriented	1.05	0.77	1.58	0.77	0.272	3.8	0.083	0.76	3.9
	90(0.38)/10 oriented	0.51	0.50	1.17	0.53	0.155	2.5	0.072	0.62	3.2
	95(0.36)/5 oriented	0.71	0.68	1.20	0.74	0.205	3.3	0.072	0.82	3.5

Conditioned at 43% RH before orientation. P—[cc(STP) cm m^{-2} atm^{-1} day^{-1}], D—[10^{-13} m^2 s^{-1}], S—[cc(STP) cm^{-3} atm^{-1}].

changed from 0.39 to 0.28 cc(STP) cm m^{-2} atm^{-1} day^{-1} as RH increased from 0 to 70% RH. The corresponding changes in P/P_{PET} were 0.41and 0.28. The same trend was observed with the oriented 95(0.36)/5 blend. The decrease in P/P_{PET} at 70% RH most probably correlated with the decrease in P_{CO2} of MXD6 at 70% RH due to tightly bound water [9], and indicated that the MXD6 domains were not completely impermeable to CO_2 at the dry condition.

4. Conclusions

This study demonstrates how the gas barrier of PET can be dramatically improved by blending with a high barrier constituent, in this case with 5 or 10 wt% of an aromatic polyamide, either MXD6 and MXD6-12I. Incorporating a small amount of sodium 5-sulfoisophthalate into the PET matrix effectively compatibilized the blends by reducing polyamide domain size. Compatibilization also inhibited crystallization of the polyamide. However, the polyamide nucleated crystallization of PET by reducing the cold crystallization temperature and increasing the crystallization temperature from the melt.

Blending 10 wt% MXD6 or MXD6-12I with PET had only a small effect on oxygen permeability of the unoriented blend, as predicted by the Maxwell model. However, biaxial orientation of the blend transformed spherical polyamide domains into platelets of high aspect ratio arrayed in the plane of the film. Increased tortuosity of the diffusion pathway, provided by the oriented platelets, reduced oxygen permeability by as much as 0.3. Analysis of oxygen permeability according to the Nielsen model indicated that polyamide domains in compatibilized MXD6 blends achieved the maximum aspect ratio of about 30 based on the draw ratio of 2.7×2.7. This result was confirmed experimentally by atomic force microscopy.

Oxygen permeability of oriented blends depended to some extent on relative humidity. The lowest oxygen permeability was measured at 43% RH; oxygen permeability was approximately 50% higher at 0% and 85% RH. The RH at which the blends were conditioned before orientation also affected the results. Hydration reduced the T_g of the polyamide and facilitated orientation of the polyamide domains. Good results were obtained with MXD6 blends conditioned at 43% RH. Due to the higher T_g of MXD6-12I, a higher conditioning RH of 85% was required to achieve optimum results with MXD6-12I blends.

Blending with MXD6 or MXD6-12I also reduced permeability of PET to carbon dioxide. Indeed, oriented polyamide domains more effectively reduced carbon dioxide permeability of PET than oxygen permeability. The typical ratio $P_{CO2}/P_{O2}=4$ of PET decreased to 3.2–3.5 for the oriented blends. This was attributed to interaction of the polar CO_2 molecule with polar groups on the polyamide.

Results observed with balanced biaxially oriented films

Table 11
Effect of RH on carbon dioxide transport parameters of biaxially oriented (2.7×2.7) PET blends with MXD6

Composition	RH	P	D	S	P/P_{PET}
PET	0	0.96	0.83	1.34	1.00
	70	1.01	0.75	1.56	1.00
95(0.36)/5	0	0.54	0.50	1.25	0.56
	70	0.45	0.39	1.34	0.45
90(0.38)/10	0	0.39	0.38	1.20	0.41
	70	0.28	0.25	1.30	0.28

Conditioned at 43% RH before orientation. P—[cc(STP) cm m^{-2} atm^{-1} day^{-1}], D—[10^{-13} m^2 s^{-1}], S—[cc(STP) cm^{-3} atm^{-1}].

were reproduced in blown bottle walls. Although the bottle was blown under different conditions of temperature and rate to an unbalanced biaxial draw ratio, the reduction in oxygen permeability achieved with 5 or 10 wt% polyamide was the same as in the films. This finding makes it possible to utilize oriented films as a model system for optimizing gas barrier of the blown bottle.

Acknowledgements

Financial support of INVISTA is gratefully acknowledged. Modern Controls, Inc. generously supported the development of a facility for gas transport studies at Case Western Reserve University.

References

[1] Kamal MR, Jinnah IA, Utracki LA. Polym Eng Sci 1984;24:1337–47.
[2] Subramanian PM. In: Koros WJ, editor. Barrier polymers and structures. Washington, DC: American Chemical Society; 1990. p. 252–65.
[3] Subramanian PM, Mehra V. Polym Eng Sci 1987;27:663–8.
[4] Lee SY, Kim SC. Polym Eng Sci 1997;37:463–75.
[5] Jarus D, Hiltner A, Baer E. Polymer 2002;43:2401–8.
[6] Kit KM, Schultz JM, Gohil RM. Polym Eng Sci 1995;35:680–92.
[7] Motta O, Di Maio L, Incarnato L, Acierno D. Polymer 1996;37:2373–7.
[8] Watanabe T. J Plast Film Sheeting 1987;3:215–34.
[9] Hu YS, Mehta S, Hiltner A, Baer E. J Polym Sci Part B: Polym Phys. In press.
[10] Turner SR, Connell GW, Stafford SL, Hewa JD. WO0109245; 2001.
[11] Al Ghatta H, Cobror S, Severini T. EP0964031; 1999.
[12] Hong K-Z, Kim YJ, Cornell SW. US5281360; 1994.
[13] Huang YQ, Liu YX, Zhao CH. J Appl Polym Sci 1998;69:1505–15.
[14] Pillon LZ, Utracki LA. Polym Eng Sci 1984;24:1300–5.
[15] Prattipati V, Hu YS, Bandi S, Mehta S, Schiraldi DA, Hiltner A, Baer E. J Appl Polym Sci. In press.
[16] Eisenberg A, Kim J-S. Introduction to ionomers. New York: Wiley; 1998. Chapter 9, p. 267–306.
[17] Wu SH. Polym Eng Sci 1987;27:335–43.
[18] Sekelik DJ, Stepanov EV, Nazarenko S, Schiraldi D, Hiltner A, Baer E. J Polym Sci Part B: Polym Phys 1999;37:847–57.
[19] Kamal MR, Sahto MA, Utracki LA. Polym Eng Sci 1982;22:1127–37.
[20] Varma DS, Dhar VK. J Appl Polym Sci 1987;33:1103–24.
[21] Nadkarni VM, Shingankuli VL, Jog JP. Polym Eng Sci 1988;28:1326–33.
[22] Tanrattanakul V, Hiltner A, Baer E, Perkins WG, Massey FL, Moet A. Polymer 1997;38:2191–200.
[23] Wunderlich B. Macromolecular physics. vol. 1. New York: Academic; 1973. p. 389.
[24] Puffr R, Sebenda J. J Polym Sci C 1967;16:79–93.
[25] Inoue K. J Polym Sci Polym Phys Ed 1985;23:743–50.
[26] Shastri R, Roehrs HC, Brown CN, Dollinger SE. In: Koros WJ, editor. Barrier polymers and structures. Washington, DC: American Chemical Society; 1990. p. 239–51.
[27] Backman A, Lange J, Hedenqvist MS. J Polym Sci Part B: Polym Phys 2004;42:947–55.
[28] Petropoulos JH. Adv Polym Sci 1985;64:93–143.
[29] Chang H, Schultz JM, Gohil RM. J Macromol Sci Phys 1967;B32:99–123.
[30] Gohil RM. J Appl Polym Sci 1993;48:1635–48.
[31] Nielsen LE. J Macromol Sci 1967;A1:929–42.
[32] Cakmak M, Spruiell JE, White JL. Polym Eng Sci 1984;24:1390–5.
[33] Del Nobile MA, Mensitieri G, Nicolais L, Weiss RA. J Polym Sci Part B: Polym Phys 1995;33:1269–80.
[34] Al-Ati T, Hotchkiss JH. J Appl Polym Sci 2002;86:2811–5.